FINAL PUBLISHABLE REPORT

Grant Agreement number	17FUN05
Project short name	PhotOQuant
Project full title	Photonic and Optomechanical Sensors for Nanoscaled and Quantum Thermometry

Project start date and duration:		01 June 2018, 42 months
Coordinator: Stéphan Briaudeau, CNAM Tel: +33 1 58 80 89 27 E-mail: Stephan.briaudeau@lecnam.net Project website address: https://www.vtt.fi/sites/photoquant/		
Internal Funded Partners: 1 CNAM, France 2 CEM, Spain 3 LNE, France 4 PTB, Germany 5 VSL, Netherlands 6 VTT, Finland	External Funded Partners: 7 CNRS, France 8 CSIC, Spain 9 IHP GmbH, Germany 10 SU, France 11 TU Delft, Netherlands 12 TUBS, Germany	Unfunded Partners:
Linked Third Parties: 13 UPD, France (linked to CNRS)		
RMG: -		

TABLE OF CONTENTS

1 Overview

This project addressed the emerging technologies for temperature sensing, particularly in scope of precise temperature measurements up to nano-scale level and in scope of their application for future dissemination of the kelvin following its re-definition in 2018. During this project, different photonic and optomechanical systems were designed, fabricated, and characterised. Calibration methods have been developed to ensure the traceability to the International Temperature Scale of 1990 (ITS-90). Photonic sensors aim at overcoming standard platinum resistance thermometers (SPRTs) drawbacks (drift, low spatial resolution, sensitivity to mechanical shocks, electromagnetic and chemical environments), while optomechanical sensors aim at providing a quantum standard for primary thermometry. This project provided a systematic study (including an uncertainty budget) of these sensors, pointing out their potential, limitations and perspectives.

2 Need

For a wide range of processes, from consumer electronics to space instrumentation, a growing need to make temperature measurements at smaller scales has been evident. The range of currently available thermometers, however, cannot meet the challenge. Nanotechnology offered the possibility of innovative 'photonic' and 'optomechanical' sensors capable of measuring temperature on micrometre length scales. Not only could these new temperature sensors replace the standard high-accuracy platinum resistance thermometers but, embedded into production processes, many industrial users could benefit from the technology. Whereas temperature is probably the most important physical variable of state, influencing almost every physical, chemical, and biological process; the world's most accurate temperature sensors, SPRTs, rely on antiquated technologies that do not lend themselves to miniaturisation, portability, or wide dissemination. Moreover, SPRTs are sensitive to mechanical shock, thermal stress and environmental variables such as humidity and chemical contaminants that cause irreproducibility and drifts. This project has developed and studied photonic temperature sensors which are inexpensive, lightweight, portable, and immune to electromagnetic interferences. Such sensors required the development of specific calibration and characterisation systems to provide traceability where usual macroscopic metrological standards were hardly applicable.

Despite their high accuracy, primary thermometers e.g. acoustic gas thermometers, dielectric gas thermometers, Johnson noise thermometers, doppler broadening thermometers) are complex and fragile thus inappropriate for dissemination purposes, whereas optomechanical devices provide a small, reliable and cost-effective primary temperature sensing method. Such sensors use zero-point motion vacuum noise as a quantised standard to scale thermal noise, and recent improvements enabled to assess the feasibility of this method at room temperature using miniaturised devices.

The high quality needed for photonic and optomechanical resonators depends on photoelastic properties of the involved materials and the losses of the guided modes. However, the existing database on photoelastic properties and losses (mechanical and optical) came from studies on bulk materials, which has been insufficient for the optimisation of the resonators used in this project and required further investigation.

3 Objectives

The overall objective of the project was to provide a quantum temperature standard for self-calibrated embedded optomechanical sensor applications, as well as optimised high resolution and high reliability photonic sensors to measure temperature at the nano and meso-scales and as possible replacement for the Standard Platinum Resistance Thermometers broadly used in temperature metrology.

The specific objectives of the project were:

1 To design and fabricate different photonic and optomechanical devices dedicated to temperature metrology at the nano- and micro-scale: photonic crystal cavities, micro-rings, micro Mach–Zehnder interferometer and membrane resonators with high optical (photonic sensors: $Q_o>10^5$; optomechanical sensors: $Q_o>10^8$) and mechanical quality factors ($Q>10^4$). A high f-Q product (f.Q>10^{12} Hz) of the mechanical resonator (product of resonance frequency and quality factor) is targeted in this project to reach quantum regime with high quantum correlations between optical and motion states.

2 To investigate the optical and mechanical performance (photo-elastic properties) of several silicon-based and diamond-based materials and their influence in the quality factor of the optical and

mechanical resonators. To study the viability of using these materials in quantum optomechanical resonators.

3 To characterise the metrological repeatability, sensitivity, and stability of both photonic and optomechanical devices, and demonstrate quantum-based read-out protocols for optomechanical devices as quantum primary temperature standards up to ambient temperature.

4 To develop methods for calibrating the developed mesoscopic sensors traceable to the practical International Temperature Scale of 1990 (ITS-90) including the evaluation of the uncertainty. The target uncertainties on temperature measurement are below 1 mK for photonic sensors and below 1 K for optomechanical sensors in quantum regime (below 10 K).

5 To facilitate the take up of the technology, developed in the project, by end users in the field of quantum and nanoscaled technology.

4 Results

Two aspects of temperature metrology were addressed in this project:

- the mise en pratique of the new (2018) definition of the kelvin unit with quantum technology using optomechanical resonators. This technology will provide a quantum temperature standard for self-calibrated embedded optomechanical sensor applications.
- the dissemination of the kelvin unit at the best uncertainty level using photonic resonators for replacing the Standard Platinum Resistance Thermometers broadly used since nearby 100 years.

The goal of this joint research project was to validate metrologically the potential of these two integrated technologies for providing nanoscale temperature sensors.

The first objective of this project was the design and fabrication of the photonic and optomechanical sensors.

The second objective was the investigation of the role of material on the performance of the sensors for their optimisation.

The third objective was the metrology study of the performance of the read-out protocol on the performance of the photonic and optomechanical sensors developed.

The fourth objective was to establish ITS-90 traceability of the developed photonic and optomechanical sensors for their metrological validation.

4.1 Objective 1: Design and fabrication of high quality photonic and optomechanical temperature sensors

The design of the sensor was the first step before its fabrication and its metrological validation.

All the sensors studied (photonic or optomechanical) use a photonic cavity. The first step was the design and fabrication of the photonic resonator of these sensors. The first requirement for reaching the high sensitivity needed for the envisioned measurements was to obtain high optical quality factors. The two kinds of resonators studied in the frame of the project (photonic and optomechanical) both need a high optical quality factor (photonic sensors: $Qo>10^5$; optomechanical sensors: $Qo>10^8$). Three different types of photonic resonators have been developed depending on the material used: silicon, silicon nitride or diamond and on the geometry (ring resonator, 1D nanobeam photonic crystal, 2D membrane).

The measurement principle being specific to the sensor technology used (photonic and optomechanical resonator), the results of this objective are split in two parts.

4.1.1 Design and fabrication of photonic sensors

Silicon ring resonators (IHP GmbH, CSIC, VSL, TUBS, PTB)

Temperature sensitivity of a photonic resonator comes mainly (99 %) from the temperature dependence of the index of refraction of its material (thermo-optical effect). Therefore, the central wavelength of the resonance of a photonic resonator is shifted with respect of its temperature. The contribution of the thermal expansion of the ring resonator is much smaller than thermo-optical effect for silicon (about 100 times smaller). Then, the temperature sensitivity of the photonic ring optical resonances depends mainly on material properties: typically

around 70 pm.K^{-1} for silicon, 30 pm.K^{-1} for gallium nitride, and 17 pm.K^{-1} for diamond following the numerical simulations computed within this project.

The temperature resolution of the photonic sensors is directly related to the spectral resolution of the reading of the resonant frequency shifting with temperature. Thus, the optical bandwidth of the resonance, which is imposed by the quality factor of the photonic resonator, is a very important parameter. Another advantage of high-quality photonic resonators is their low optical losses i.e. low self-heating caused by two photon absorption of the optical power of the probe laser.

The quality factor of a ring resonator depends on its optical losses including the coupling rate and absorption, but it also depends on the group index (propagation velocity of the light power) of the material and the radius of the ring. Nevertheless, the role of ring radius on the quality factor is not obvious as optical losses caused by absorption increase with ring radius.

Following a pragmatic approach, the dependence of the quality factor with these parameters has been studied systematically and experimentally. A large number of silicon ring resonators has been designed and fabricated with different ring radius, group index value, but also gap distance (200 nm to 500 nm) separating the ring resonator from the optical waveguide (optical coupling through evanescent wave) which drives the coupling rate to the ring resonator.

Finite element Multiphysics simulations have been performed for design optimisation, in collaboration between partners. These numerical simulations consider linear and nonlinear optical absorption, photothermal, thermal and mechanical properties. It allows to evaluate self-heating and the temperature induced shift of the optical resonance wavelength. These simulations have been computed on silicon micro ring resonators with SiN cladding. The conclusions of these simulations have allowed the optimisation of the ring resonators following a feedback process between simulation, design, fabrication and characterisation.

Thus, the photonic resonators have been designed following a standardised Photonic Integrated Circuit (PIC) process. The fabricated chips include over 100 ring resonators, thus enabling the optimisation of their quality factor depending on their design parameters (ring radius, gap, waveguide dimensions).

An optical grating has been also designed to facilitate the optical coupling from the optical fibre to the input port (optical waveguide) of the ring resonators. It also reduces the sensitivity of the optical coupling to mechanical vibrations of the fibre tip used compared to front face coupling. The laser light propagating in this optical waveguide is then injected into the photonic ring resonator from evanescent wave optical coupling through a tiny gap.

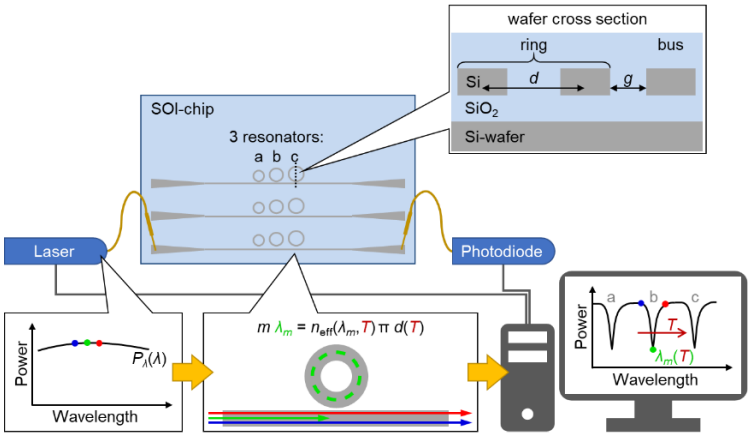

Figure 1: explanation of the temperature measurement principle using photonic ring resonators. A cw monomode tunable laser is coupled into the PIC with optical fibre alignment. The transmitted laser power is then collected with an optical fibre, measured with a photodiode whose signal is sampled for spectral analysis. The PIC chipset integrates many ring resonators for the systematic study of their response to temperature, depending on their design parameters.

The fabrication process provides a layout data translated into mask data. Available etching levels ranges from 70 to 220 nm with smallest features size being 130/130 nm. The process uses deep UV (248nm) and i-line scanner, dry and wet etching, Chemical-Mechanical Polishing, CMP, implantation deposition and epitaxy techniques.

This optimisation process based on the collaboration of several partners on simulation, design, fabrication and characterisation stages have allowed to reach high quality factors up to 200 000 measured on Si ring resonators. It corresponds to a narrow (0.008 nm) optical bandwidth of the Notch resonance at telecom (NIR)

optical wavelength (ranging from 1525 to 1565 nm). Such performance has been obtained with an optimum gap of 500 nm with ring resonators having a radius of 35 μm. This combination corresponds to a critical coupling from the optical waveguide to the ring resonator (equal reflected power and coupled power). Such critical coupling also generates very high contrast (20dB) Notch resonances providing a high signal to noise ratio. These resonators have been shared among three partners which have studied the devices with different experimental setup and optical interrogation schemes.

Diamond ring resonators (CSIC)

Among other material candidates, diamond is promising for both photonic and optomechanical resonators as its absorption (linear and two photons) is very small compared to standard materials (Si, Si_3N_4), providing much smaller unwanted self-heating.

Currently, temperature sensors (Si microrings) reported by NIST have limitation due to self-heating problems due to two-photon absorption. Diamond does not have two-photon absorption in this wavelength range, so it is a promising material. Besides, it has excellent thermal conductivity. Despite the resonance shift for diamond photonic resonator is smaller due to its smaller thermos-optic coefficient, the overall performance could be better in terms of noise and accuracy. Diamond is also optimum for high frequency optomechanical devices due to its high Young´s Modullus (1 MPa).

Nevertheless, the main difficulty with diamond, was the lack of knowledge of processing technology existing at the beginning of this project. A procedure has been developed to fabricate diamond photonic crystal membrane using polycrystalline diamond deposited by high pressure Chemical Vapour Deposition on SiOx layer on Si buffer. The removal of the SiOx layer liberated the membrane. The fabricated membrane was fabricated with holes forming a 2D quasi periodic structure to generate photonic confinement. The quality factor of this diamond photonic membrane was limited by high roughness level (10 nm peak to peak) which is the main issue with diamond process.

A dual material (GaN and diamond) integrated photonic sensor has then been designed and fabricated.

A GaN racetrack photonic resonator (65μm length, bend radius 30μm) is coupled to a diamond microdisk (diameter 25 μm, thickness 1.8 μm). This ensemble of two coupled photonic resonators provides a hybrid device which exhibits GaN and diamond Notch sharp resonances at telecom wavelength (1540-1600 nm) having an optical bandwidth of 0.035 nm (i.e. quality factor about 100 000).

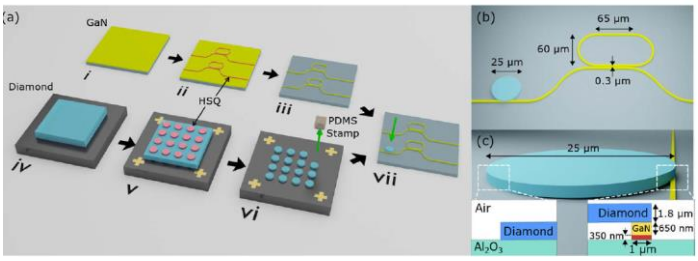

Figure 2: The parallel process flow: (i) The GaN wafer is (ii) patterned with HSQ e-beam resist and (iii) etched in an ICP-RIE using Ar/Cl2 chemistry. (iv) The diamond is thinned to ~ 1μm - 2μm , also with an Ar/Cl2 ICP etch before being (v) transferred to a silicon chip pre-patterned with e-beam alignment markers, whereupon HSQ is spun and patterned into disks. (vi) An Ar/O2 ICP etch down to the silicon exposes the disks, before a disk of thickness 1.8 μm is (vii) transfer printed on to the GaN chip. (b) Device dimensions. (c) Cross-sectional dimensions, showing a total waveguide height of 1 μm consisting of 650 nm of GaN and 350 nm of AlN buffer layer.

4.1.2 Design and fabrication of optomechanical resonators

Optomechanical resonators are made of a mechanical resonator coupled to a photonic resonator so that thermal fluctuations of the mechanical resonator are transduced into fluctuations of the optical resonator for optical reading.

Going along with a high optical quality factor, high mechanical quality factor is also compulsory for optomechanical resonators. For these structures, both optical and mechanical modes, with their respective high-quality factors, should also have a strong coupling. This so-called optomechanical coupling, overlap between the optical and the mechanical field, has been optimised with Finite Element Methods (F.E.M.). In order to reach high transduction between photons and phonons, one of the project's targets was to reach state of the art values of the resonance frequency, around or above a few megahertz.

The vacuum optomechanical coupling strength, g_0 expressed as a frequency, quantifies the interaction between a single phonon and a single photon: it corresponds to the optical frequency shift induced by the zero-

point fluctuation amplitude of the mechanical oscillator. In the case of optomechanical photonic crystals, mainly two mechanical effects can contribute to the optical frequency shift and thus to g_0. These effects are the moving interface effect and the photoelastic effect.

Another key feature for optomechanical resonators is the f-Q product (f being the mechanical resonant frequency and Q the mechanical quality factor), the product of mechanical resonance frequency and quality factor. To be able to perform quantum experiments at room temperature, the f-Q product has to be larger than 10^{12} Hz.

Two strategies have been pursued in the frame of this project to reach these high f-Q products, either by using a diffraction-limited cavity with a mechanical resonance frequency in the GHz or by drastically decreasing mechanical losses (anchor losses and thermo-elastic damping).

Nanobeam optomechanical resonator with high mechanical frequency (GHz) (CNRS, SU, CSIC)

Suspended photonic crystals use the total internal reflexion along at least one dimension (two for the nanobeams) in order to confine light. The high index contrast between the material and the surrounding air guarantees the spatial confinement over this axis, the other two being imposed by the photonic crystal. This configuration is particularly useful for realising optomechanical devices as the suspension introduces the needed mechanical degree of freedom. One strategy for realising PhC microcavities consists in the insertion of defects in a well-defined PhC structure. The crystal must be designed such that the desired resonance frequency lies in the photonic band gap. Then, by artificially inserting a defect in the crystal definition, one locally allows the light to propagate in the material at a frequency originally forbidden. By engineering the photonic crystal design as well as the defect, it possible to create extremely localised photonic modes showing high optical Q-factor. This strong confinement is at origin of many nonlinear light-matter interactions, including radiation pressure forces used for cavity optomechanics experiments.

In 1D photonic crystal nanobeams, the optical field is confined by total internal reflexion along two directions. The defect can be introduced via the apodization of the design. This consists in smoothly changing the hole shapes, the crystal spacing or the hole sizes towards the centre of the microcavity. From a more technical point of view, the cavity is built in the nanobeam by piercing a 1D-photonic crystal made of holes into which the lattice constant is subtly varied. This strategy for the optical confinement has been followed for a 200 nm thick Si_3N_4 membrane. A 1D-photonic crystal membrane with a fundamental resonance at 865nm and an optical Q-factor of about 2.10^6 has been achieved.

Figure 3: (Bottom) photonic crystal design
. (Top) Electromagnetic field distribution at 865 nm with an optical Q-factor of about 2.10^6.

Once the design with high Q-factor at the targeted wavelength is achieved, mechanical properties can be computed with a Finite Element Model software. In this case, the main properties which need to be known are the mechanical properties of material namely Si_3N_4. The fundamental mechanical mode is at 6.4 GHz with a displacement field distribution shown in Figure 4. The mechanical quality factor is estimated $Q=2.5\ 10^5$. The computed effective mass is equal to $2.5\ 10^{-16}$ g. The strong localisation of the mechanical mode in the same region as its optical counterpart creates a strong optomechanical coupling. For the photonic crystal design, the total optomechanical coupling g_0=4 MHz.

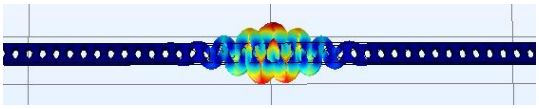

Figure 4: Field distribution of the fundamental mechanical mode of the 1D photonic crystal nanobeam made of Si_3N_4 at 6 GHz.

The optomechanical crystal investigated by CNRS and SU is based on a suspended 200 nm thick membrane of silicon nitride (Si3N4) over silicon wafer.

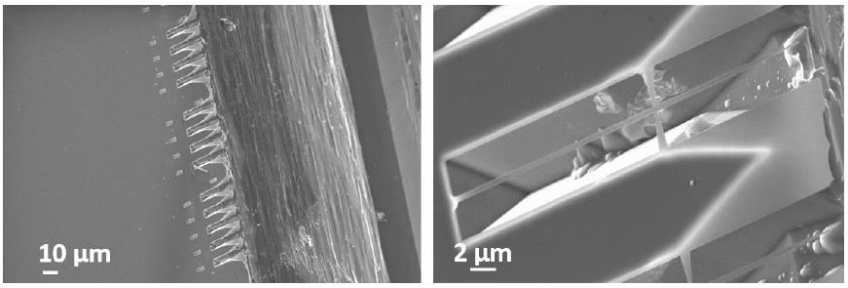

Figure 5: (left) Scanning Electron Microscope image of the sawing of sample with several devices on the edge of the chip. (right) Zoom on one suspended optomechanical crystal made of Si3N4.

Membrane optomechanical resonator with high quality factor (Q>10^6) (TU Delft)

One of the most successful implementations of mechanical oscillators for optomechanics are membranes made of high-stress silicon nitride (Si_3N_4). The high tensile stress is indeed known to decrease the intrinsic losses in the material, phenomena known as dissipation dilution, leading to extraordinary high values of the mechanical quality factor. Engineering the stress in the resonators allows one then to confine the stress in desired regions and further dilute the dissipation.

The optomechanical resonators developed at TU Delft are suspended membranes fabricated from 200 nm and 50 nm thick high-stress (1.3 GPa) Si_3N_4 deposited by low pressure chemical vapour deposition (LPCVD) on a Si support. The resonators are patterned with a phononic crystal to reduce the bending at the clamping points and increase the mechanical quality factor.

Based on those works, the chosen mechanical resonator is a 2D phononic crystal with a local irregularity of the phononic lattice in the centre. The defect is designed to have an eigenfrequency inside the acoustic bandgap of the surrounding phononic crystal. By doing that, the eigenmode of the defect is spatially confined in the centre of the membrane and the bending curvature near the clamping point is strongly suppressed, resulting in an increase of the mechanical quality factor.

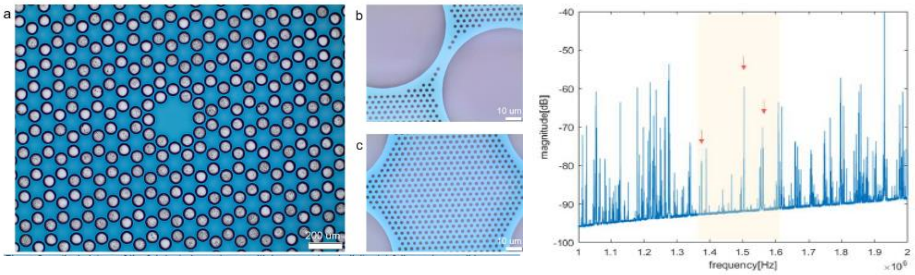

Figure 6: Left: optical picture of the fabricated membrane with hexagonal periodicity. (a) full membrane, (b) zoom on the tether area, (c) zoom on the pad area. Right: measured spectrum in the central part of the membrane. The yellow area highlights the bandgap and the red arrows the confined modes in it.

The fabricated resonators have been characterised using Doppler vibrometer spectrum of membrane with hexagonal periodicity, in Figure 6, showing an acoustic bandgap in good agreement with the simulation from 1.4 MHz to 1.6 MHz. 3 confined modes, highlighted with a red arrow, are visible in it. The bandgap contains also additional resonance frequencies coming from the substrate or the measurement setup.

A quality factor of 1.2 10^5 is obtained at a vacuum level 10^{-3} mbar whereas the losses are dominated by air damping. Operating at a pressure of 10^{-8} mbar is needed to neglect any contribution from gas damping and measure the intrinsic quality factor of the fabricated resonators. A new interferometer with high vacuum chamber (10^{-8} mbar) capability has been built. Using this experimental setup, the mechanical resonance frequency was measured at 900 kHz and a mechanical quality factor exceeding 10^8, leading to an f.Q product of 710^{14} Hz, 35 % lower than the highest reported f.Q product for SiN resonators. The presented result is obtained with a 50 nm thick Si_3N_4 layer.

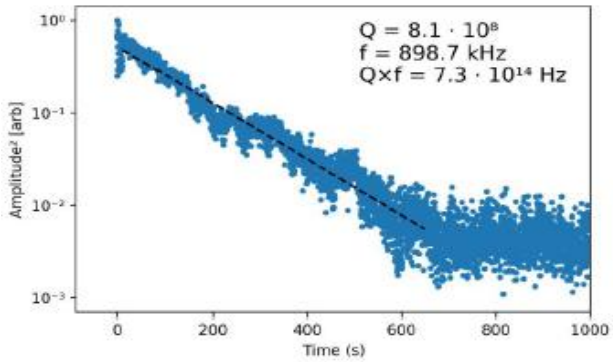

Figure 7: ringdown measurement of a string resonator obtained by driving the resonator with a piezoelectric actuator at the resonance frequency. At t=11 seconds the drive is then shuttered off and the displacement recorded with a spectrum analyser.

Key outputs and conclusions of objective 1:

Strong collaborative efforts have been made to push the performance of photonic and optomechanical sensors into state-of-the-art quality criteria, following complementary strategies for a most effective approach: materials (silicon, diamond, SiN, GaP), geometries (ring resonators, nanobeam, square membrane), mechanical frequencies (from MHz to GHz). Silicon ring resonators have shown the best performance whereas processing technique remains the main limitation for high quality diamond photonic resonator. The SiN square membrane optomechanical sensor has demonstrated the potential of 2D geometry whereas GaP nanobeam has experimented large self-heating caused by residual optical absorption and poor thermalisation. The objective 1 has been successfully achieved.

4.2 Objective 2: Investigation of device materials for functional optimisation (TUBS, PTB, IHP GmbH, CSIC, CEM, VTT, CNRS, TU Delft)

The partners investigated several material aspects and their impact on the performance of photonic and optomechanical temperature sensors. The aim was to compare the properties of materials used for photonic and optomechanical devices. For the material properties of photonic devices, this involved studies of birefringence, estimation of self-heating effects and scattering induced by surface roughness as well as mechanical losses. The investigations served as feedback particularly for the design of photonic temperature sensors based on optical microring resonators.

Within the project different materials for photonic microring resonators were evaluated with respect to their use in temperature sensing. The focus on the evaluation was on silicon, silicon nitride and diamond. Additionally, temperature sensitivity and absorption losses (and their impact on the feasible quality factor and self-heating) were also theoretically studied for germanium and gallium nitride devices. Germanium may be of future interest due to its extremely high temperatures sensitivity and gallium nitride for its compatibility to III-V semiconductor processes and potentially less self-heating than silicon. To compare the different materials, the partners chose the criteria temperature sensitivity, optical losses & self-heating, wavelength range, and availability of high-performance devices & technology maturity. The investigations focused on an operation temperature of or around 300 K.

To study the temperature sensitivity of microring resonators consisting of different materials numerical simulations based on finite element method (COMSOL Multiphysics) were utilised in different 2D and 3D implementations being all in good agreement with experimental data. Hereby, the focus was on models that require low computational resources and provide fast results.

Of all considered materials that can be utilised at the telecommunication wavelength of 1550 nm silicon provided the highest temperature sensitivity. It was found to be about a factor of 4 larger than the sensitivity of comparable resonators made of diamond or silicon nitride. It is twice as high as the sensitivity for an optical ring resonator made of gallium nitride. With values between 60 and 80 pm/K the high temperature sensitivity of silicon was experimentally confirmed. To this end, silicon microring resonators with different geometries, i.e. rib waveguides and wire waveguides have been realised by the partners. From the experimental data the photothermal properties of the systems could be determined, e.g., a silicon thermo-optic coefficient of 1.85E-4/K was retrieved for silicon.

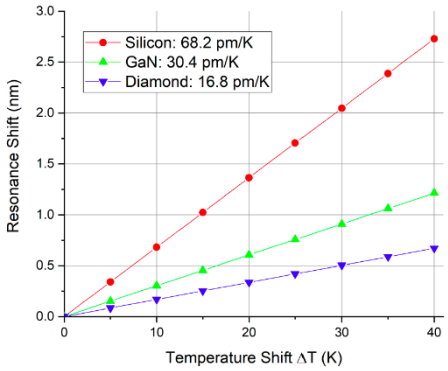

Figure 8: Computed sensitivities of ring resonators made of Si, gallium nitride (GaN) and diamond around 1550 nm using the axis-symmetric model. Reference temperature for the thermo-optic coefficient is room temperature (from Weituschat, L.M.; Dickmann, W.; Guimbao, J.; Ramos, D.; Kroker, S.; Postigo, P.A. Photonic and Thermal Modelling of Microrings in Silicon, Diamond and GaN for Temperature Sensing. Nanomaterials **2020**, 10, 934).

The experimental results and their very good agreement with predictions by finite-element simulations (COMSOL Multiphysics) illustrated the excellent performance of silicon with respect to temperature sensitivity. For instance, the effective refractive index of fabricated wire waveguides was experimentally determined to be 2.48 whereas with COMSOL Multiphysics a value of 2.4805 was retrieved. Thermal expansion and photoelastic effects may (as secondary effect) induce additional shifts of the resonance wavelengths. Additionally, hysteresis effects can occur. Silicon, diamond and silicon nitride have similar thermal expansion coefficients. The photoelastic coefficient of diamond (-0.272) measured within this project was found to be a factor of 2 larger compared to silicon (-0.114) and silicon nitride rendering diamond slightly disadvantageous in this regard.

CSIC has designed in collaboration with PTB optical microring resonators made of different materials (silicon, diamond and gallium nitride) and simulated their temperature behaviour using several finite-element methods. The temperature sensitivities of the designed devices have been simulated numerically (16.8 pmK^{-1} for diamond, 68.2 pmK^{-1} for silicon and 30.4 pmK^{-1} for GaN, see Figure 8). In addition, the influence of two-photon-absorption (TPA) and the associated self-heating on the accuracy of the temperature measurement have been analysed. The results show that owing to the absence of intrinsic TPA-processes self-heating at resonance is less critical in diamond and GaN than in silicon.

The partners also studied the influence of optical losses on the performance of photonic temperature sensors. Optical losses induced by absorption and scattering are critical for the performance of microring resonators due to two major aspects: 1) they limit the feasible optical quality-factors, and 2) they lead to self-heating. Self-heating is detrimental for the signal-to noise ratio and may result in asymmetries in the resonance peaks. Within the project quality factors of up to 1.7E5 were achieved with optical microrings based on silicon illustrating that for silicon the material quality that is feasible with semiconductor technology enables high quality factors. For large circulating powers that are easily reached in such systems, also two-photon absorption (TPA) plays an important role. The two-photon absorption coefficient of silicon is 8E12. Due to their larger bandgap, TPA is negligible for silicon nitride and diamond and gallium nitride, as well. To investigate self-heating, the partners developed a semi-analytical model that allows for an easy distinction of geometry related influences and material related influences, respectively. The model was established for microring resonators and microdisc resonators. The studies were performed for silicon, gallium nitride, silicon nitride and diamond in dependence of the circulating light power. The results showed that self-heating in diamond turned out to be much less critical than in silicon. This is due to the higher absorption in silicon and due to the excellent thermal conductivity of diamond. For example, at a circulating power of 1 mW self-heating in diamond was found to be a factor of about 4 smaller than in silicon and GaN, respectively.

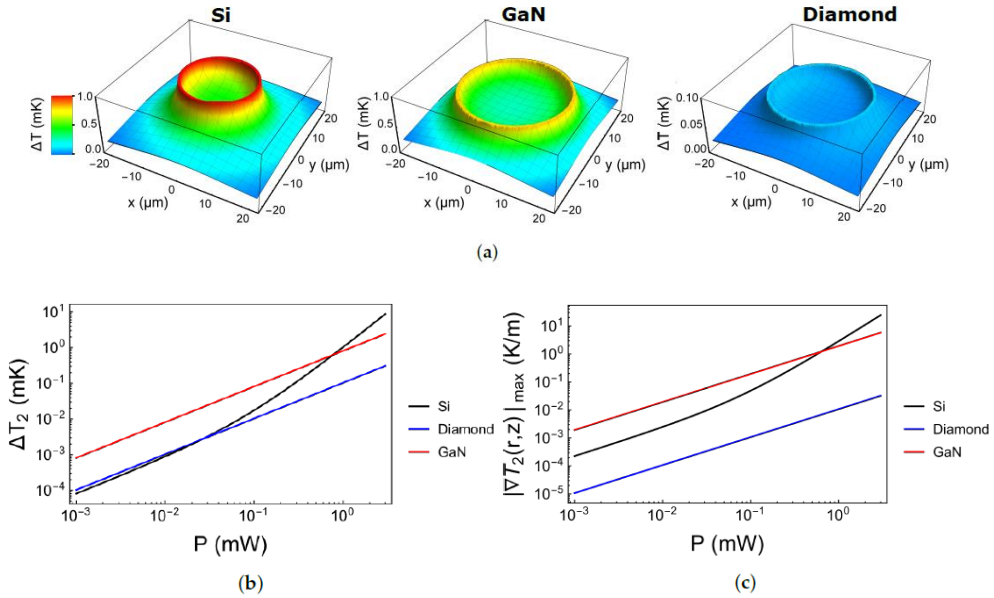

Figure 9: (a) Calculated temperature fields in the Si, GaN and diamond resonators with a power of P=1 mW. (b) Calculated mean temperature increase in the ring resonators as a function of the circulating power for Si, diamond and gaN. (c) Calculated maximum gradient of the temperature field in the ring resonators as a function of the circulating power for Si, diamond and GaN.

As another potentially important indicator for the performance and behaviour of optical microring resonators the maximum gradient of the temperature field in the resonator was evaluated. It corresponds to stress induced (photo-elastic) refractive index changes. Diamond was identified as superior in this regard due to its very high thermal conductivity. However, the resulting temperature difference within the resonator was only about mK in Si for P = 1 mW which is about three orders of magnitude smaller than the self-heating itself. Thus, temperature gradient effects can be expected less critical for the device performance. A similar situation is found when microdisc resonators instead of microrings made of different materials are considered. Mainly due to a better thermal contact to the substrate the overall self-heating is about a factor of 2 smaller for all materials. The results gained by the various modelling techniques also supported the understanding of experimental results including effects like asymmetries in the resonance peaks shape and spectral shifts of the resonances.

In another activity, the partners developed a completely analytical model for spatially and temporal temperature fields (and thus self-heating effects) in air-cladded optical microring resonators (ORRs). For that purpose, the heat equation boundary value problem under continuous excitation was solved in air-cladded ORRs. The self-heating effect was explicitly calculated for a widely applied ORR technology platform: a silicon ring resonator on a silica glass bottom cladding. More explicitly, this ORR was produced using a multi-project wafer prototyping process. Experimentally determined parameters were included in the calculations.

It was shown that the heating amplitude, which was about 50 mK for an input power of 1 mW, was mainly determined by the bottom cladding due to its small thermal conductivity. Excitation times for reaching half of the equilibrium temperature increase were in the range of a few µs, and therefore about 104 times larger than typical charge carrier lifetimes in the resonator ring. As expected, the heating amplitude rises linearly with the input power in the linear absorption dominated and quadratically in the TPA dominated regime. In the latter power range (here above a threshold of about 14 mW), optical bistability effects caused significant asymmetries in the resonance shape. The analytical results were also verified by rigorous finite element simulations (FEM) in thermal equilibrium. For this purpose, the software COMSOL Multiphysics was utilised. Both analytical and numerical results were in good agreement down to a deviation of about 20 % in the heating amplitude and of about 55 % in the TPA threshold. Those deviations could be attributed to a simplification in the analytical model, namely a homogeneous intensity distribution in the ring.

The derived equations enable the determination of the whole temperature field with drastically reduced computational effort compared to FEM simulations, enabling fast scans over large whole parameter spaces. In future, the derived analytical model shall be extended by charge carrier dynamics and optical bistability effects. That extension would enable the modelling of absorption induced resonance distortions at low computational costs.

The results on self-heating effects showed that the self-heating amplitude is approximately proportional to the total absorbed power and anti-proportional to the thermal conductivity of the cladding material. Further, two-photon absorption plays a major role in the heating process, even for moderate input powers, due to the strong light confinement. Heating times were determined to be in the microsecond range and may limit the response time of ORR devices. The explicit formulas for the temperature fields developed within this work allow a much faster determination of heating properties compared to elaborate finite element simulations. Thus, the developed model is predesignated for scanning large parameter spaces.

Concluding, the results retrieved within the project and available literature data illustrate that all three materials, silicon, diamond, and silicon nitride, are suitable for photonic temperature sensors enabling sufficiently large quality factors. Particularly, silicon and silicon nitride impress with their highly advanced production technology and a combination/integration with optomechanical devices seems to be feasible soon with standardised processes on an industrial level. Due to its excellent thermal conductivity and the absence of TPA in the wavelength of interest diamond-based devices will suffer less from self-heating effects.

In addition to purely photonic systems, the partners also investigated the influence of different material parameters for optomechanical temperature sensing. Also here, silicon, silicon nitride and diamond were compared. Depending on the specific device design some of the aspects studied for photonic sensors also apply for optomechanical sensors. Particularly, if optical modes with high quality factors are utilised self-heating will be as relevant as for photonic sensors.

To compare the feasible Q-f product for optomechanical systems made of different materials several mechanisms inducing mechanical losses were evaluated such as clamping losses, thermoelastic dissipation (TED), phonon tunneling and the Akhiezer effect. To this end the partners set up multiphysics simulations based on finite element method. Effects like hermal transport and energy loss based on heat transfer were modeled for diverse device geometries and dimensions (e.g. membranes, beams, trampolines) and (temperature dependent) material properties. These results were compared to measurements on devices purchased by commercial providers and fabricated within the project. The measurements were caried out by exciting the oscillators with noise and measuring the mechanical ring down of the excited modes. As an exemplary result, at room temperature the mechanical loss of silicon nitride was computed to be about a factor of ten larger than that of silicon and diamond for the same membrane geometry. Reducing the thickness of the devices reduces the TED losses. A similar situation was found for rectangular beams clamped on two ends and trampoline structures. For beams and membranes made of silicon TED was confirmed to be the dominating loss at room temperature. Qualitatively, it could also be shown that less clamping area (2 edges in comparison to 4 edges) enable better performance in terms of Q-f values in low-stress materials. With high-stress SiN membranes a Q-f product of up to 1.4E10 was measured.

As an upper limit for the feasible Q-f product Akhiezer damping arising from quantum mechanical phonon processes was studied. In conventional device geometries, the comparatively small thermal conductivity of SiN compared to silicon and diamond would render SiN less favourable to achieve ultra-high Q-f products. However, it has been shown that even this limit can be overcome by device engineering combining the dilution effect in stressed silicon nitride with phononic shielding. That way, Q-f products as high as 1.4E14 have been achieved.

As another device configuration within the project optomechanical sensors based on microdisc resonators were studied. To quantify the interaction between the optical and mechanical mode, i.e. the optomechanical coupling, in such systems photoelastic material parameters were characterised in dependence of temperature. To this end an optical polarimetric setup was utilised to analyse the polarisation state of light after passing sample of the respective material. The sample was placed in a cryostat. By applying defined mechanical load, the stress induced birefringence was retrieved. The contribution of the photoelastic properties to the overall optomechanical coupling scales linearly with the photoelastic coefficients of the material and with the fourth power of the refractive index. For, instance, at room temperature the photoelasticity of diamond was measured to be twice as high as for silicon nitride and silicon. Assuming equivalent electric and mechanical field distributions in the device the difference in the refractive index would lead to an optomechanical coupling that is highest for silicon structures.

Based on the results within the project and literature data, the partners consider silicon and silicon nitride devices for optomechanical temperature sensing mature regarding the related technology and existing know-how. High performance devices based on silicon and silicon nitride have been already successfully demonstrated. The high tensile stress that can be realised for silicon nitride devices is beneficial for fabricating high aspect ratio membranes which would collapse without it and thus enhancing the design flexibility to realise

ultra-sensitive sensing devices. Several high-frequency optomechanical devices have been demonstrated using diamond but their final use as temperature sensors has not been explored, yet. The ultimate limits in terms of the Q-f product seem to be a little more restrictive for silicon than for silicon nitride and diamond even though the diamond technology needs further technology development. Diamond has very low optical absorption and could circumvent problems due to self-heating. Since silicon nitride is already well established for both photonic and optomechanical devices it is a very attractive material to go towards integrated photonic-optomechanical systems that could cover large temperature ranges.

Key outputs and conclusions of objective 2:

The characterisation of photo-elastic material properties and mechanical loss investigations on silicon, silicon nitride and diamond have been finalised. In addition, photothermal properties have been successfully extracted from transmittance measurements in silicon photonic microring resonators. These experimental activities have been complemented by numerical and semi-analytic modelling of self-heating due to material absorption. All the results served as a basis for the material comparison illustrating the excellent properties of silicon devices in mass production with state-of-the-art technology and the potential of silicon nitride and diamond for thermometry approaching fundamental limits. The objective 2 has been successfully achieved.

4.3 Objective 3: Development and study of optical read-out techniques for photonic and optomechanical sensors

Optical reading of temperature with optomechanical and photonic sensors requires the development and the study of dedicated read-out protocols to define their limiting factors and the attached systematic errors. As the two kinds of sensors use different measurement principle, this objective is split into each sensor type.

4.3.1 Read-out protocol for photonic sensors (PTB, VTT, VSL, CSIC, CEM)

This section is dedicated to the study of photonic sensor technology around room temperature (from 5°C to 95 °C). The measurement principle is based on the thermo-optical effect: the optical wavelength at resonance depends on the temperature. The refraction index of the optical resonator depends on temperature but also its size (thermal expansion).

The measurement principle of temperature using a photonic sensor made of an optical resonator whose refractive index n and length L both depends on temperature (T). The wavelength of the optical resonance thus depends on the temperature. The resolution of the resonance reading is thus of first importance for this sensor and high-quality optical resonators are necessary for high resolution of the optical reading of the resonant optical wavelength. For silicon ring resonators, the sensitivity is about 72 pm.K^{-1} so that a temperature uncertainty about 1 mK around room temperature is equivalent to an uncertainty on the reading of the resonant optical wavelength about 0.07 pm with a resonant optical wavelength within C-band telecom optical wavelengths.

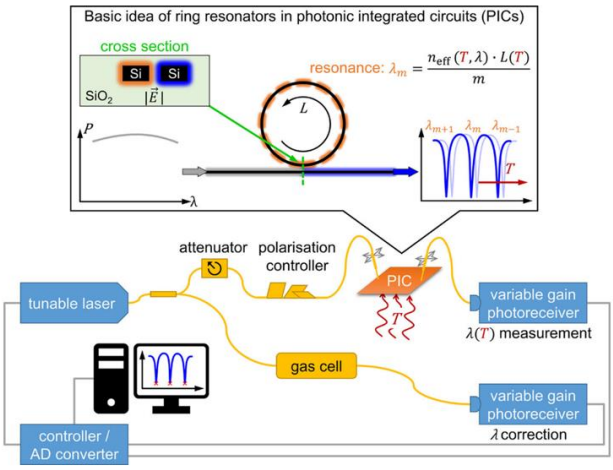

Figure 10: Setup for photonic thermometry. A cw monomode tunable laser is coupled into the PIC with optical fibre alignment. The transmitted laser power is then collected with an optical fibre, measured with a photodiode whose signal is sampled for spectral analysis. The PIC chipset integrates many ring resonators for the systematic study of their response to temperature, depending on their design parameters. .(R. Eisermann, S.Krenek, G.Winze, S. Rudtsch, tm – Technisches Messen 2021; 88(10): 640–654)

The probe laser is guided via glass fibres to the silicon waveguides. This fibre-coupled optical path additionally contains a variable attenuator and a polarisation controller. Both elements are adjusted manually to reduce possible self-heating, and polarisation dependent effect is minimised. The fibre-to-chip coupling is achieved by using two microstructured planar grating couplers. The transmitted spectrum passing through the PIC is guided to variable gain photoreceivers. The light guidance of the PIC structures with subwavelength size results from the refractive index contrast between the silicon waveguide and the surrounding oxide. A second circular waveguide (ring resonator) is evanescently coupled to the bus waveguide and works as an optical cavity.

To reach this target, the optical quality factor of the sensor is pushed to state-of-the-art value ($Q=1.5\ 10^5$) so that Half Width at Half Maximum is about HWHM=5 pm. The wavelength resolution required is thus reduced to a fraction of 1.4% of HWHM which becomes a reasonable target taking account for noise detection limitation (< 0.1% /√Hz). Nevertheless, using high-quality factor optical resonator produces high optical power per unit area inside the optical waveguide. Above a fraction of a mW, the optical power of the incident laser beam generates nonlinear (two-photon) optical absorption which produces non negligible self-heating inside the ring resonator. For this reason, the optical power is restricted below 0,1 mW.

The optical wavelength (around 1550 nm) of the probe laser is of first importance. It has been determined with two different techniques. The first technique uses a reference gas cell of hydrogen cyanide ($H^{13}C^{14}N$) at a pressure of 3.3 kPa providing reference lines for calibrating the laser wavelength. It enables fast measurement (MHz sampling rate) together with fast tuning of the laser wavelength (100 $nm.s^{-1}$). A complete spectrum (60 nm spectral width) may then be recorded within 1 s (more than 100 samples within the optical resonance full width at half maximum: 10 pm). The standard uncertainty attached to this technique has been estimated about 0.6 pm. Finally, the noise limitation of the ring resonator prototype has been measured, depending on the measurement bandwidth. Smallest temperature standard deviation (0.01 mK) has been reached with a measurement time about 1 sec. Such low standard deviation is related to the laser wavelength uncertainty (0.01 pm), at the level of the best commercial lasers locked on molecular frequency references.

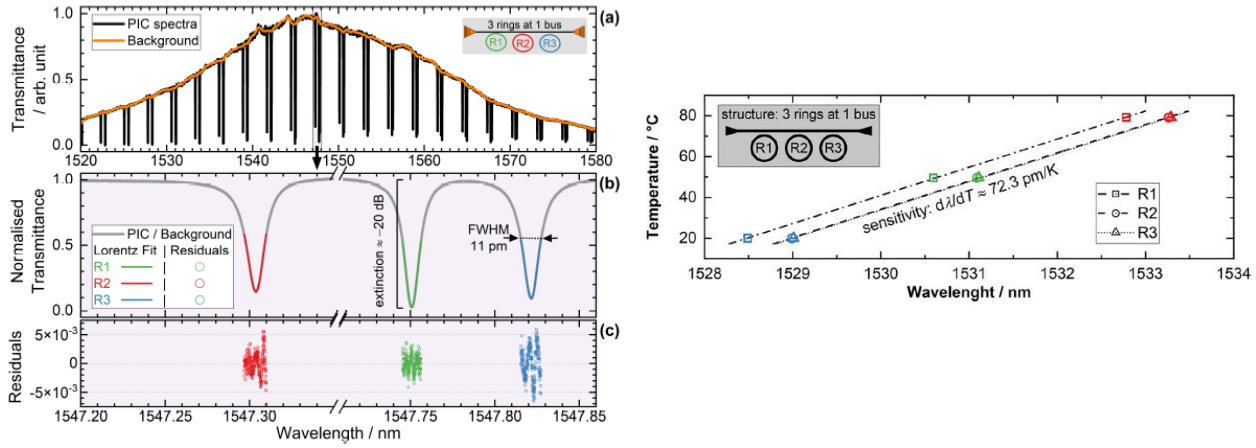

Figure 11: Data processing of the photonic integrated circuit spectra with 3 ring resonators (a) Raw data of Photonic Integrated Circuit transmittance and estimated background arising from grating coupler and optical setup. (b) Optical resonances normalised. A Lorentz fit of the peak region is used to determine the exact position of the resonance centre wavelength. (c) Residuals of the fits. .(R. Eisermann, S.Krenek, G.Winze, S. Rudtsch, tm – Technisches Messen 2021; 88(10): 640–654)

4.3.2 Read-out protocol for optomechanical sensors (TU Delft, CNAM, LNE, CNRS, SU)

Two measurement principles have been studied for temperature measurements with optomechanical resonators:

- Spectral shift of the resonant optical frequency with temperature
- Optomechanical Noise Thermometry

Two read-out techniques have been studied for optomechanical noise thermometry

- Side-of-fringe transduction of phase noise into intensity noise
- Optical homodyne detection of phase noise

Photonic thermometry with optomechanical sensors

Optomechanical sensors contain an optical resonator coupled to a mechanical resonator. The read-out protocol studied with photonic sensors may also be applied to optomechanical sensors. The consortium has studied the temperature shift of the optical resonance of an optomechanical resonator. The read-out protocol of the resonant optical wavelength followed. Optical characterisation of the 1D Optical Crystal has been performed with the fibre setup shown in Figure 12. The sample is inserted into a circulating liquid helium cryostat at a low pressure (few mBar) of helium exchange gas. The copper sample holder is equipped with three calibrated resistive temperature sensors to estimate both bulk and surface temperature to identify any temperature drop between the sensor and the bulk temperature measured. The white light of a superluminescent light emitting diode (SLED) is injected and collected back with a lensed fibre and analysed with an Optical Spectrum Analyser (0.01 nm wavelength accuracy). The alignment is performed with a 3-stage micropositioners and monitored from the outside of the cryostat with a camera mounted on a microscope, as shown in Figure 12. The studied resonators exhibit optical modes in the IR C-band telecom wavelength range $\lambda \simeq 1550$ nm, with optical quality factors $Q \approx 10\,510$.

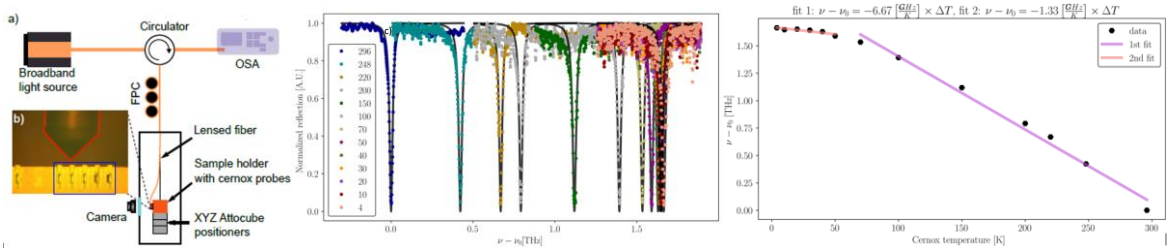

Figure 12: Optical setup and photonic results with 1D nanobeam optomechanical resonator. a) Schematic of the photonic characterisation setup. A broad light source (SLED) is used to align the sample with respect to the fibre using a XYZ attocube micropositionners. The reflected signal is detected on an optical spectrum analyser (OSA). b) Image from the alignment camera, the fibre is outlined in red and the samples in blue. c) Optical resonance frequency shift due to thermorefractive and thermal expansion effects.

Figure 12 shows several optical spectra, each of them being recorded at a temperature ranging from 100 K to 300 K. Each curve has been fitted with a Lorentzian line shape, from which optical frequency $\nu_0(T)$ was extracted and plotted against the temperature variation (T). The temperature slope S = −6.58 GHz/K is in a good agreement with associated literature on GaP nanobeam optomechanics. The frequency resolution of the OSA (6.6 GHz) is then equivalent to a temperature resolution of 0.7 K. The SLED power on optical resonance remains below 100 nW so that self-heating caused by optical absorption is negligible.

Noise thermometry with optomechanical sensors

Once the optical resonator of the optomechanical sensor has been characterised, optomechanical noise-thermometry technique has been studied and applied to optomechanical sensors. This technique is similar to Johnson noise-thermometry (J.N.T.), whereas it is not sensitive to electromagnetic noise.

Thermomechanical noise is caused by the Brownian thermal motion at a given temperature, associated with an average kinetic energy per degree of freedom equal to $E_k = k_B.T/2$. The mechanical resonator is then thermally excited with a broadband random force. At thermal equilibrium, the variance $\overline{x^2}$ of the mechanical vibration is written $\overline{x^2} = \frac{k_B.T}{k_{eff}}$ with ω_m the resonant mechanical pulsation, m_{eff} the effective mass of the mechanical mode whose stiffness k_{eff} follows: $k_{eff} = \omega_m^2.m_{eff}$.

Thanks to optomechanical coupling, the optical phase φ of the probe laser field is correlated to the mechanical displacement “x”: $\overline{\varphi^2} = \frac{1}{L}.\frac{\omega_0}{\omega_m}\overline{x^2}$ with ω_0 the optical pulsation and L the optical length of the optical cavity. The effective mass “m_{eff}” of the studied mechanical mode is needed for the determination of the temperature.

The first read-out technique implemented, but also the simplest, is called “side-of-fringe”. Thanks to optomechanical coupling, the thermal noise is transduced into optical phase noise which is itself converted into optical intensity noise. The conversion factor is given by the slope of the optical resonance spectrum for a given detuning. Thus, the maximum sensitivity of the “side-of-fringe” technique is reached at half-width optical detuning. The optical intensity noise is measured with a fast photodiode. Then an electrical spectrum analyser provides the so-called mechanical noise spectrum. Due to the very high sensitivity of the optical alignment of the probe laser to the optomechanical sensor for their coupling, the sample must be realigned with respect to the fibre after each temperature change. Therefore, the optical transduction cannot be kept invariant while the temperature is varied. Consequently, this reduces the reproducibility of the side-of-fringe technique. The optical

phase of the probe laser beam is modulated, at a pulsation Ω_{mod} in the vicinity of the mechanical pulsation ω_m so that the tone experiments the same transduction than the mechanical thermal noise. The mechanical spectrum is normalised with respect to the calibration tone, yielding a ratio of the photodiode signal noise power to the tone power. This power ratio R_T is proportional to the temperature T:

$$T = \left(\frac{R_T}{R_{296\,K}}\right).296\,K$$

with $R_{296\,K}$ the power ratio recorded at room temperature (296 K).

Measurement results with 1D nanobeam optomechanical sensor

Temperature measurements with 1D optical crystal have been realised with the fibre setup depicted in Figure 13a. The light source is a cw telecom tuneable laser whose frequency is set at the edge of the optical mode's resonance at half width detuning. The laser probe power is kept small to prevent from nonlinear self-oscillation regime. Therefore, the optical power of the reflected laser beam is so low that it must be amplified with an erbium-doped fibre amplifier (EDFA) for a photodiode signal being larger than the electrical noise floor.

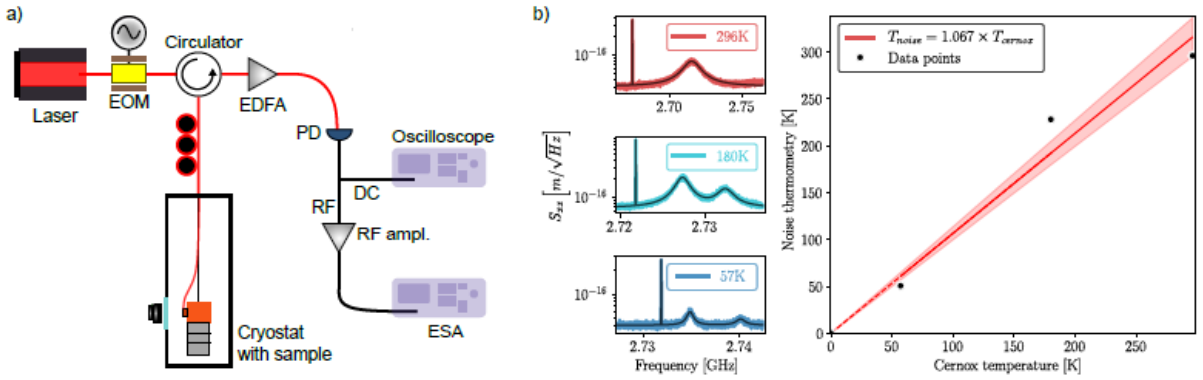

Figure 13: a, Schematic of the calibrated noise thermometry measurement setup. The optomechanical crystal is placed in a 4He cryostat. The acquisition of the Brownian motion spectra, via the electrical spectrum analyser (ESA) relies on the side of fringe measurement scheme. EOM: Electro-optical phase modulator. FPC: Fibered polarisation controller. EDFA: Erbium-Doped Fiber Amplifier. PD: High-speed photodiode. b, Left: Brownian motion spectra with their calibration tone at different temperatures. Right: Extracted temperature from the ratio of the areas of the Brownian motion and calibration peaks. The red curve is a linear fit to the extracted data.

This measurement technique has been validated with resistive thermal probes (Cernox) which have been calibrated against ITS-90 references (Figure 13b). The three recorded data points have been fitted with a linear function.

The high (GHz range) resonance frequency of the 1D ladder mechanical resonator is required for quantum correlation read-out technique at room temperature. As a counterpart, the level of thermal noise scales as ω_m^{-2}. It is 1 million times larger with MHz mechanical frequency sample. The optical coupling of the probe laser to the 1D ladder inside the cryostat requires the use of microlensed optical fibre which exhibits non negligible optical losses. Therefore, only a small fraction of the incident laser power is reflected by the optomechanical resonator before being detected. The value of the probe laser power required for the mechanical resonance being above the electronic noise level was about few 10µW. At this level, the optical absorption generates self-heating which modifies the index of refraction of light and generated optical bistability: the spectral shape of the optical resonance shape becomes triangular. The side of fringe detection technique is preliminary but not competitive for high performance optomechanical noise thermometry.

Measurement results with 2D square membrane optomechanical sensor

Square membrane optomechanical resonator has been studied with side of fringe technique. This 2D optomechanical resonator is complementary to the nanobeam. Its resonant mechanical frequency is much lower (MHz range) thus the amplitude of the mechanical vibrations is expected to be 1 million times larger than that observed with 1D nanobeam. The 2D geometry of the mechanical resonator enhances thermal conduction and lowers self-heating. The mechanical displacement is probed using a He:Ne laser (632.8 nm) and the mechanical resonator is mounted inside a cryogenic vacuum chamber. The sample holder is equipped with an ITS-90 calibrated thin film resistance temperature sensor, for SI traceability of the temperature measurements. The light is then focused on the sample, and it is partially reflected by the suspended silicon nitride membrane, partially transmitted to the underneath silicon substrate and reflected by it, creating a Fabry-Perot cavity. The

interference between the different light paths results in a position dependent light intensity that is used to determine the membrane's motion. The reflected light is then focused on the photodiode, connected to a spectrum analyser which allows to extract the Brownian motion. As expected, the measured power spectra $S_{VV}(\omega)$ and its spectral integral giving the mechanical displacement $\langle x^2 \rangle$, exhibit a clear dependence on the temperature of the resonator which is also measured with contact resistance sensor calibrated with ITS-90 references and methods. This last step allows to obtain the conversion factor from the measured power spectra $S_{VV}(\omega)$ to the position power spectra $S_{xx}(\omega)$. The spectrum acquired at each temperature can be fitted by the model of the mechanical resonance having parameters (effective massm_{eff} quality factor Q_m and resonance pulsation ω_m and the temperature T). Finally, the temperature of the resonator is calculated by integrating the fitted curve $S_{xx}(\omega)$ and obtaining the mechanical displacement $\langle x^2 \rangle$.

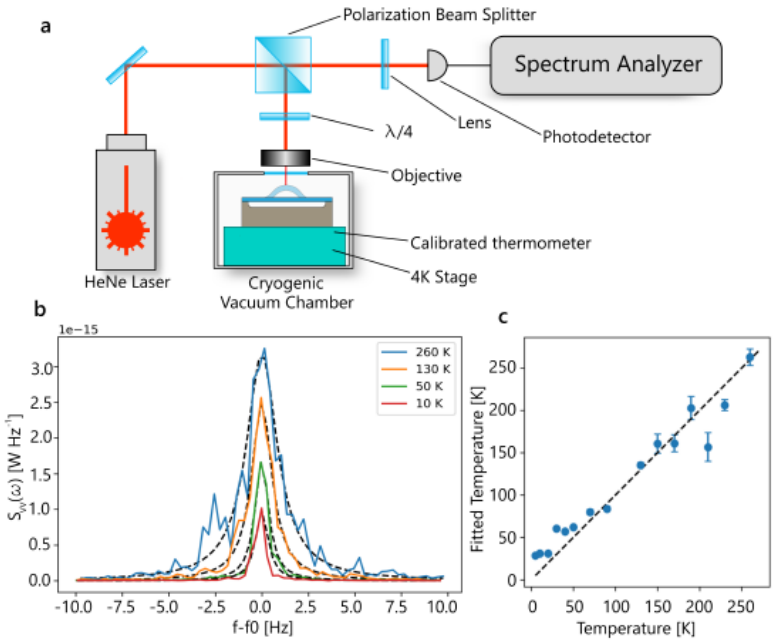

Figure 14: (a) Schematic of the mechanical characterisation setup. The mechanical resonator is placed inside a cryogenic vacuum chamber and the displacement caused by Brownian notion is detected optically via a spectrum analyser. (b) Thermomechanical noise spectra at different temperatures with a spectrum analyser. The x.axis is centred at the resonance frequency of each spectrum for comparison. (c) Temperature extracted from the measurements in (b) by integrating the area under the peak. The error bars show the standard deviation.

At each temperature, the focus on the sample is adjusted to ensure a comparable sensitivity over the entire temperature range. We note that this procedure can introduce additional uncertainty in the conversion factor, which should be eliminated in the final implementation of the thermometry protocol, e.g. using a calibration tone as described for the 1D nanobeam device. Figure 14c shows the fitted temperature for each measurement, compared to the temperature of the resonator obtained from the independent calibrated commercial sensor. The error bars indicate the standard deviation for each measurement. This result shows reasonable agreement between the optical noise thermometry method and the temperature obtained from the independent calibrated sensor over the range of 5 K to 260 K, providing evidence for the potential of the described thermometry technique. Due to the small linewidth and peak-height at low temperatures the error bars and uncertainty in the optomechanical noise thermometry increase at low temperatures, causing deviations from the temperature obtained from the independent calibrated sensors. The positive deviation of the temperature at low might partly be attributed to a systematic overestimation of the peak area by the employed fitting routine.

Key outputs and conclusions of objective 3:

As a conclusion the objective 3 has been mostly achieved. The photonic devices have been metrologically fully characterised (repeatability, sensitivity, and stability). The optomechanical devices were only characterised in the noise thermometry read-out protocol. The following systematic effect had to be solved before attempting to use quantum correlation for quantum primary thermometry: optical bistability caused by optical absorption in GaP nanobeam optomechanical resonator but also the residual amplitude modulation caused by the electrooptical phase modulator used to provide a calibration tone for optomechanical noise thermometry.

4.4 Objective 4: Development of methods for calibrating the developed mesoscopic sensors traceable to ITS-90

The aim of this objective is to develop methods for the metrological validation of photonic and optomechanical thermometers, which will be done by calibration of the developed mesoscopic sensors traceable to the International Temperature Scale of 1990 (ITS-90) and evaluation of the calibration uncertainty. This objective requires the design and the fabrication of thermostats having high temperature stability and high temperature homogeneity. The thermostat design also depends on the temperature range. The temperature range for the study of photonic sensors is restricted from 5 °C to 95 °C, with an accuracy of 1mK. It allows using open air thermostats made of a sample holder (plate) stabilised in temperature using a circulating fluid. The temperature range for the study of optomechanical sensors extends from 5 K to 300 K with an accuracy ranging respectively from 1mK (@ 4K) up to 1K (@ 300 K). It requires the use of a closed cryostat.

4.4.1 Systematic effects and uncertainty budget for photonic thermometry from 5 to 95 °C (PTB, VSL, VTT, CSIC, CEM)

Thermostat

The experimental setup of the PTB is based on fibre coupling of the laser light via a micrometre air gap and coupling gratings on the photonic chip. For the thermostat this means that the fibres had to be positioned very precisely over the chip (accuracy and stability below 100 nm). Therefore, this thermostat is based on a temperature-controlled platform that is connected to a conventional water thermostat (Figure 15).

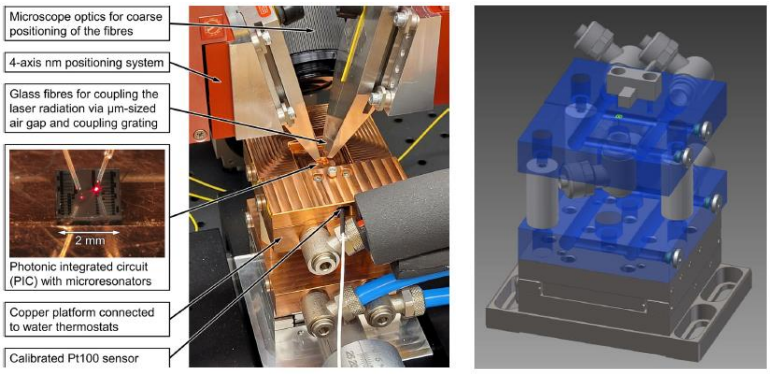

Figure 15: Experimental setup to characterise photonic resonators at PTB. .(R. Eisermann, S.Krenek, G.Winze, S. Rudtsch, tm – Technisches Messen 2021; 88(10): 640–654)

The design of the thermostat platform is based on the following considerations:

• In order to ensure the temperature of the surface is as homogeneous as possible a copper block with optimised water flow was designed. The water flows around the centrally positioned chip on all sides.

• To ensure stable positioning of the chip and good thermal contact with the thermostat platform, the chip is held in place by a vacuum tweezers through a small hole. The chip can be easily aligned parallel to the symmetry axis of the measurement setup through a small edge on the surface of the platform.

• In order to maintain the high positioning accuracy even at changing temperatures, the temperature-controlled platform must be thermally isolated from the positioning unit below it. For this purpose, another platform is mounted on the positioning unit, through which water flows at a constant temperature. Both platforms are connected to each other by ceramic spacers, so that thermal expansion and heat transfer are minimised.

Temperature stability

Two thermostats in series show the best stability of the surface temperature, with standard deviations between 0.7 mK and 7.4 mK for a duration of 30 min in the entire temperature range from 10 °C to 90 °C. Additionally, the long-term stability was investigated for 30 °C, which results in a standard deviation of approximately 2.6 mK for a duration of 24 h. Over this period, no drift of the surface temperature was detected. As described in 4.3.1 the high spectral scanning speed, achieved by wavelength traceability by reference gas cells, allows measurement times quite below 10 s. The relevant short-term stability is in most cases below 0.5 mK to 4 mK, increasing from room temperature to 90 °C.

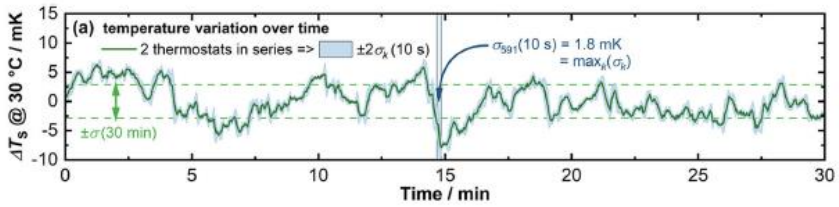

Figure 16: Temperature variation of the surface temperature of the thermostat platform determined at 30 °C for 30 min for the two thermostats in series .(R. Eisermann, S.Krenek, G.Winze, S. Rudtsch, tm – Technisches Messen 2021; 88(10): 640–654)

Optical coupling stability

Other possible uncertainty source is the fibre coupling configuration. A small air gap is used for the characterisation of the integrated photonic circuit. To ensure an optimal power coupling between the input/output optical fibre and the photonic gratings, the positioning with submicron accuracy in all three axes, including the angle of the fibres is crucial. With changing temperatures of the temperature-controlled platform, the relative position between the fibre tip and the chip can change due to thermal expansion of the copper platform and the steel fibre holders. Therefore, the coupling fibres were raised between the individual temperature steps and readjusted in the temperature plateaus. Relative coupling changes were determined for different temperatures. The measurement condition is similar to the determination of spectral transmission, except that the wavelength was kept constant at 1550 nm (outside the ring resonance).

The relative transmitted power exhibits a standard deviation of power changes over the measurement time of 10 s: from 0.2 % at 20 °C to 1.0 % at 90 °C.

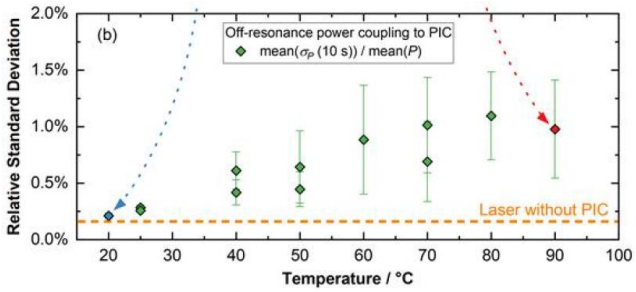

Figure 17: Optical coupling stability for a nominal thermostat temperature of 20 °C and 90 °C for a 100 s long measurement: mean standard deviation corresponding to 0.1 Hz measurement bandwidth. .(R. Eisermann, S.Krenek, G.Winze, S. Rudtsch, tm – Technisches Messen 2021; 88(10): 640–654)

Measurement noise

For long time intervals of several minutes and more, the temperature fluctuations of the thermostat temperature are the dominant temperature noise source. Within the duration of a single measurement (from 0.1 sec to 10 sec), the dominant uncertainty (8 mK) is related to the wavelength calibration of the spectrum (0.006 nm) caused by fluctuations of the resonant optical wavelength during the laser scan. The lock of the laser wavelength to a single resonance in a constant power mode may be used to shorten the measurement time, thus, reducing the fluctuations of the resonant optical wavelength.

Another relevant factor for constant power operation (resonance locking) is the coupling stability and the associated fluctuation in the transmission. Due to the thermal fluctuations, the coupling between the fibres and the PIC changes. Consequently, the transmission noise including the PIC is higher and increases with increasing temperature noise even for the PIC off resonance. Since the photonic resonator itself is temperature-sensitive, the transmission noise is higher compared to off-resonance. The transmission noise for the on-/off-resonance is comparable for higher sampling rates (>1 Hz).

Uncertainty budget: photonic thermometry

A complete uncertainty budget has been provided by PTB for photonic thermometry. The uncertainty is mainly imposed by the calibration of the resonant optical wavelength (8 mK) and by the traceability to ITS-90 (8 mK). For more details see: https://doi.org/10.1515/teme-2021-0054

Source	Value	Uncertainty Contribution (k = 1) / mK
Temperature-Controlled Platform (mean + 2σ of short-term standard deviations, see Fig. 4)	0.46 mK @ 20 °C	0.46 @ 20 °C
	4.2 mK @ 90 °C	**4.2** @ 90 °C
ITS-90 calibration of Pt100	8.2 mK	8.2
Wavelength stability (see Fig. 12)	<3.6 fm	<**0.05**
Wavelength calibration (typical standard deviation, see Fig. 9)	600 fm	**8.2**
Resonator peak fit, including coupling stability from Fig. 5 (mean + 2σ of peak difference standard deviations, see Sec. 4.1)	300 fm	**4.1**
Packaging (ageing or drift), T_{chip} vs. T_{Pt100}, $T(\lambda)$-fit (see text)	Unknown	Unknown
Repeatability (includes bold printed values)		≤**10**

Table 1: Summary of the discussed uncertainty contribution within a typical measurement interval of 10 s for the swept wavelength based photonic thermometry sensing method. (R. Eisermann, S.Krenek, G.Winze, S. Rudtsch, tm – Technisches Messen 2021; 88(10): 640–654)

4.4.2 Systematic effects and uncertainty budget for optomechanical thermometry from 4 K to 300 K (CNAM, LNE, VSL, SU, TU Delft)

Thermostat

The aim of optomechanical thermometry is to provide a primary temperature sensor, studied from 1.5 K up to 300 K. Such a large temperature range requires the use of a cryostat which must provide optical access (optical window and optical fibre) for laser coupling to the sensor through optical fibre. The very small area (100 nm x 400 nm) of the input aperture of the optical waveguide of the optomechanical resonator requires high numerical aperture optics together with nm resolution of the position. The use of a microscope objective inside the cryostat is not possible, due to the small size of the cryostat chamber. It is replaced by a microlensed (10 micrometre focal length) optical fibre. A three-axis translation stage with nm resolution is then required for theoretical alignment of the lensed fibre in front of the optical waveguide. Due to differential thermal expansion of the fibre and sample holders, the optical alignment must be re-adjusted following any temperature change greater than 10 K. A 20x magnification imaging system, located outside the cryostat, views the optomechanical resonator and the microlensed optical fibre through an optical window for their preliminary optical alignment.

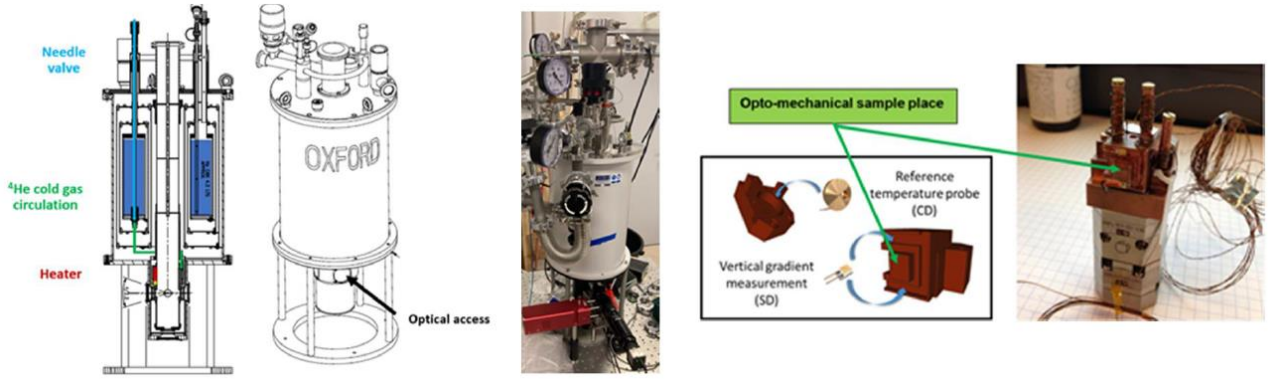

Figure 18: Left: Schematic of the ^{4}He cryostat. Middle: Picture of the cryostat with its tubing and mounted on the experiment table. Right: Copper assembly mounted on XYZ nanopositionners.

Three contact, electrical resistor probes are used for temperature traceability and measurement of any possible thermal gradient. These three electrical resistor sensors have been calibrated against International Temperature Scale of 1990. One temperature sensor is located inside the sample holder to provide “bulk” temperature while the two other temperature sensors are located at the surface of the sample holder, close to the optomechanical resonator. Any thermal gradient at the surface of the sample holder of the so-called temperature drop between surface and bulk temperature may then be estimated with sub 100 mK resolution.

Temperature traceability: uncertainty budget

The self heating, calibration, thermal gradient, thermal stability and uncertainty relative to the measurement of electrical resistor are presented in the table below. The uncertainty of the temperature traceability ranges from 17 mK @ 4 K to 105 mK @ 300 K.

Source	Components	at 4 K	at 300 K
Cernox	self-heating	< 15 mK	< 15mK
	calibration	3 mK	92 mK
Measurement scheme	ref. resistance value	negl.	3 mK
Cryostat	gradient	5 mK	40 mK
	stability	4 mK	25 mK
Uncertainty, mK	**k=1**	**17 mK**	**105 mK**
Uncertainty, mK	**k=2**	**33 mK**	**209 mK**

Table 2: uncertainty budget of temperature traceability using contact Cernox Probes

Systematic effects

Any thermometer experiments self-heating caused by its interaction with the probe physical quantity. As an example, electrical resistor temperature sensors are subject to Joule heating. Thus, this systematic effect has to be estimated. The self-heating of optomechanical resonators is caused by optical absorption originating from material optical properties (linear absorption, nonlinear two-photon absorption) or imperfections of the fabrication technique (material impurities, surface roughness). Thermal heat is dissipated through the mechanical clamps between the optomechanical resonator and the substrate. The self-heating has then been studied on both geometries (2D membrane and 1D nanobeam) which have been developed by the partners.

Self-heating with 1D nanobeam

In the following, the thermal contribution of the probe's optical power absorption on the 1D optical cavity was estimated. This estimate relies on an optomechanical static non-linear effect equivalent to a Kerr effect where the refractive index of the material depends on the optical power. This leads to a deformation of the optical resonance when scanning the laser wavelength and could even end up in an optical bistability. In our case this phenomenon is likely induced by the absorption of light circulating inside the optical cavity that causes a temperature increase of the optomechanical crystal and changes in the refractive index. This behaviour is presented in Figure 19 where, at medium input power, the optical resonance leaves the Lorentzian shape and shows a more and more triangular shape where the resonance frequency is shifted toward low frequency. At high input power, the resonance even exhibits a bistable behaviour with a rapid drop just after reaching the resonance frequency. All curves in Figure 19 are obtained by sweeping the laser from high to low frequency. When sweeping the laser frequency up, hysteresis can be observed for the curves obtained at 100 and 200 µW. The minima of each curve of Figure 19 have been extracted and plotted against the input power pin. A linear fit of the data points gives a shift coefficient equal to α_{rad} = 0.025 K / µW. The temperature variation ΔT is then estimated by combining this frequency shift and the shift coefficient obtained in Figure 12c. The resulting heating induced by optical absorption is depicted in Figure 19: it varies linearly with the optical power.

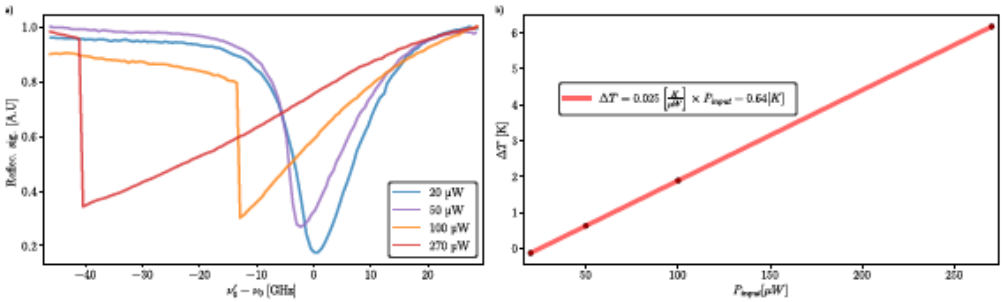

Figure 19: Bistability of the optical resonance frequency with increasing input power. a: Evolution of the Lorentzian optical mode into a bistable one with increasing power. The frequency shift of the local minima of each curve of Figure 19a is converted into temperature drop using frequency shift coefficient depicted in Figure 12c. It is then plotted against input power (Figure 19b).

Self-heating with 2D membrane

The spatial distribution of the temperature in the 2D membrane has been numerically simulated using COMSOL Multiphysics software and a finite elements model. The physical properties (thermal, optical and mechanical) of the membrane's material have been taken from literature. The laser beam profile has been taken as gaussian, located at the centre of the membrane while the temperature of its outer boundaries is set to 5 K. The result in Figure 20.a shows a localised temperature increase in the centre of the 2D square membrane of 0.18 K at an incident laser power of 65 µW, the highest value employed in the measurement. The laser power absorbed by the SiN membrane is 0.65 µW, 1 % of the incident power. The localised laser

heating and associated temperature increase have a three-fold effect on the developed noise-thermometry scheme: the resonance frequency decreases as a result of the tension induced by thermal expansion, the area under the position noise power spectrum increases and the signal on the photodiode increases due to the larger conversion factor at higher laser power. Figure 20c shows the change in resonance frequency as function of incident laser power, where a linear relation can be observed as expected.

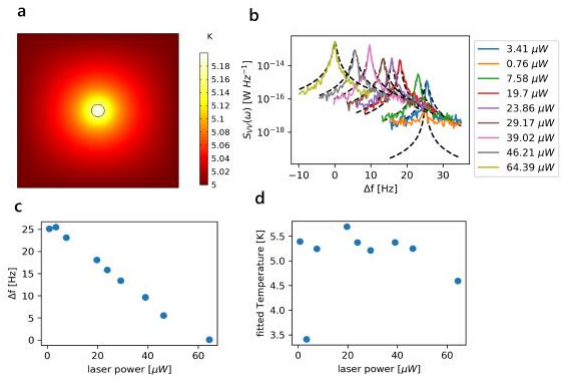

Figure 20. a, Simulated temperature distribution plot with an incident power P=65 μW. b, Thermomechanical noise spectra measured at a temperature of 5 K for different laser powers. The x axis is the difference in frequency from the resonance frequency measured with a laser power of 65 μW, equal to 1.3 MHz. c, Measured resonance frequency difference versus laser power with respect to the resonance frequency acquired with a laser power of 65 μW. d, temperature extracted from the measurements in b) by integrating the area under the peak versus laser power.

The resonance frequency can be an accurate measure of temperature, that might complement noise thermometry protocols for reaching higher precision temperature measurements, while using thermomechanical noise for accuracy and self-calibration. In Figure 20d, the temperature at every laser power was determined using noise thermometry, by integrating the fitted area under the peaks in Figure 20b. Prior to the fits shown in Figure 20b, an additional thermomechanical calibration step is performed for all the spectra, providing for each laser power a conversion factor from voltage Power Spectrum Density (PSD) to position PSD.

Key outputs and conclusions of objective 4:

As a conclusion, the objective 4 was mainly achieved in terms of the developed methods for ITS-90 traceable calibration of the new sensors. The photonic thermometry and photomechanical noise thermometry have been demonstrated but their associated uncertainties still stand above the project target values: 12 mK uncertainty for photonic sensor around room temperature and 10 K uncertainty for the optomechanical sensor (photothermal noise thermometry) from 4K to 300 K.

Conclusion

Experimental studies have been realised on a variety of photonic and optomechanical thermometers, demonstrating different sensing and calibration approaches. With the photonic devices a very high temperature sensitivity of 81 pm/K has been demonstrated, and 10 mK uncertainty has been achieved around room temperature. Photomechanical noise thermometry on nanomechanical devices was applied to measure temperatures over the range from 5 K to 300 K. A single calibration temperature has been used to determine thermodynamic temperature over the whole temperature range. The first uncertainty budget associated to photomechanical noise thermometry exhibited a 10 K uncertainty.

5 Impact

The project results have been presented at 16 European and international conferences (e.g. CPEM 2018, EQTC 2019, TEMPMEKO 2019, SMSI 2020, Graphene & 2D Materials Industrial Forum 2021, GSELOP2021) and at EURAMET TCT meetings (May 2018, April 2019, September 2020). The project partners are involved in the task group of the Comité consultatif de thermométrie (Emerging technologies). Four meetings of the stakeholder committee have been held on the occasions of preparation of 1st report in Madrid in February 2019, 2nd report in Delft in November 2019, 3rd report (online meeting) in December 2020 and final report in Berlin (hybrid meeting) in November 2021. Based on the activities presented by the partners during the reporting meetings, newsletters have been prepared and distributed within the stakeholder committee and other interested parties. Also, an online International Workshop has been organised at the end of the project in order to exchange knowledge and introduce the project results to the international scientific community involved in this field (external researchers from USA and China have also presented their research). The

consortium produced 14 peer reviewed articles / proceedings, out of which are 12 published thus far. A final summary with the project results has been published in MPDI Optics 2022: "Photonic and Optomechanical Thermometry" https://www.mdpi.com/2673-3269/3/2/17/pdf. The project information and links to the publications and the presentations can be found on the project website (https://projectsites.vtt.fi/sites/photoquant/publications.html).

Impact on industrial and other user communities

The photonic sensors developed in this project (objective 4) shall provide a solution to *in-situ* temperature measurement in harsh environments such as high energy particles, nuclear irradiation, chemical species) and high resolution. The optomechanical noise thermometry has been demonstrated whereas the temperature uncertainty (few K) was still limited by some systematic effects for industrial applications. Nevertheless, technical solutions to the systematic effects have been identified, for their test in near future.

Future on-chip optical communication applications face major issues with temperature management and require localised temperature measurements. With metrologically validated photonic sensors that are distributed over the silicon chip, one can envision more accurate power distribution and temperature control. Another rapidly growing product is the power transistor, more ubiquitously used for converting electric power in applications ranging from mobile phone chargers and solar panels to electric cars. Heat generation in these transistors causes thermomechanical stresses that can lead to dangerous short circuits that can cause fires or explosions in battery-driven applications. Accurate, distributed temperature sensors can prevent these failures and their related dangers.

Impact on the metrology and scientific communities

The measurement of thermodynamic temperature has been pushed to its ultimate performance for the determination of the Boltzmann constant and the forthcoming redefinition of the kelvin. This collaborative research project was the first European attempt to develop a quantum standard for temperature metrology. The developed optomechanical sensors provide first primary temperature sensors of easy access to end users. This project also paved the way to high accuracy temperature measurement on a mesoscopic scale. With an improved robustness and sensitivity, photonic sensors could replace standard platinum resistance thermometers.

The metrological characterisation of photo-elastic material properties and mechanical loss investigations on silicon, silicon nitride and diamond shall have a strong impact on scientific community as it provides a physical model and a material database for designing the process of high-performance ring resonators sensors.

Impact on relevant standards

The performance and reliability of the new type of sensors developed in this project and their potential in terms of robustness (compared to Standard Platinum Resistance Thermometers) in the realisation of a practical temperature scale have been discussed on CCT Task Group for Emerging Technologies (CCT-TG-CTh-ET) in October 2020. The viability of optomechanical sensors as new primary thermometers and their inclusion in the mise-en-pratique for the definition of the kelvin has been also discussed.

Longer-term economic, social and environmental impacts

A wider impact of the sensors developed within this project is foreseen in the field of metrology as the sensors based on quantum standards may renew thermometric methods in future years. As such sensors do not require any calibration against standard artefacts, metrological skills will shift from calibration services to sensor integration and expertise on systematic effects. Nowadays, the uncertainty attached to photonic and optomechanical sensors is still limiting their impact on temperature metrology. Photonic sensors could also replace the platinum resistance thermometers so widely used in process control or inspection at present. These primary thermometers operating at mesoscopic scale may push advances in biology research, health, environment and nuclear safety. The demonstration of the viability of these sensors in thermometry will also open the way to their use in other metrology fields as pressure or nano-force measurements.

Developed photonic devices can be used for temperature control in harsh environment for microprocessor production process, high power transistors, telecommunications. Optomechanical sensors shall be competitive at cryogenic temperature for absolute temperature determination: below 1K, the magnitude of thermal noise becomes comparable to quantum noise floor. Thus, the performance of optomechanical sensors in quantum entering quantum regime should be enhanced towards absolute zero kelvin.

6 List of publications

Jingkun Guo, Richard A. Norte, Simon Gröblacher, "*Feedback cooling of a room temperature mechanical oscillator close to its motional groundstate*", Physical Review Letters 123, 223602 (2019), DOI: https://doi.org/10.1103/PhysRevLett.123.223602; https://arxiv.org/abs/1911.01586

Lukas Weituschat, Walter Dickmann, Joaquín Guimbao, Daniel Ramos, Stefanie Kroker, Pablo Aitor Postigo, "*Photonic and Thermal Modelling of Microrings in Silicon, Diamond and GaN for Temperature Sensing*", Nanomaterials 2020, 10(5), 934; https://doi.org/10.3390/nano10050934

S. Krenek, R. Eisermann, S. Rudtsch , G. Winzer and T. Habisreuther, "*Photonic Thermometry at PTB – Challenges and Perspectives for Contact Temperature Metrology Utilizing Optical Sensors*", SMSI 2020 - System of Units and Metrological Infrastructure, pages 360 – 361, https://doi.org/10.5162/SMSI2020/E1.4

T. Briant, S. Krenek, A. Cupertino , F. Loubar, R. Braive, L. Weituschat, D. Ramos, M. J. Martin, P. A. Postigo, A. Casas, R. Eisermann, D. Schmid, S. Tabandeh, O. Hahtela, S. Pourjamal, O. Kozlova, S. Kroker, W. Dickmann, L. Zimmermann, G. Winzer, T. Martel, P. G. Steeneken, R. A. Norte and S. Briaudeau. MPDI Optics 2022: "*Photonic and Optomechanical Thermometry*" https://doi.org/10.3390/opt3020017

Chen, X., Kothari, N., Keskekler, A., Steeneken, P.G. and Alijani, F., 2022: *"Diamagnetically levitating resonant weighing scale*", arXiv arXiv:2105 (2022) , 1-16, https://doi.org/10.48550/arXiv.2105.12444

Chen, X., Keskekler, A., Alijani, F. and Steeneken, P.G., 2022: "*Rigid body dynamics of diamagnetically levitating graphite resonators*", arXiv arXiv:2006 (2022), 1-6, https://doi.org/10.48550/arXiv.2006.01733

Eisermann, René, Krenek, Stephan, Winzer, Georg and Rudtsch, Steffen. "*Photonic contact thermometry using silicon ring resonators and tuneable laser-based spectroscopy*" tm - Technisches Messen, vol. 88, no. 10, 2021, pp. 640-654. https://doi.org/10.1515/teme-2021-0054

Robin J. Dolleman, Debadi Chakraborty, Daniel R. Ladiges, Herre S. J. van der Zant, John E. Sader, and Peter G. Steeneken, "*Squeeze-Film Effect on Atomically Thin Resonators in the High-Pressure Limit",* Nano Letters 2021 21 (18), 7617-7624. https://doi.org/10.1021/acs.nanolett.1c02237

Elías Ferreiro-Vila, Juan Molina, Lukas M. Weituschat, Eduardo Gil-Santos, Pablo A. Postigo, and Daniel Ramos, "*Micro-Kelvin Resolution at Room Temperature Using Nanomechanical Thermometry*", ACS Omega 2021 6 (36), 23052-23058. https://doi.org/10.1021/acsomega.1c02045

Jack A. Smith, Paul Hill, Charalambos Klitis, Lukas Weituschat, Pablo A. Postigo, Marc Sorel, Martin D. Dawson, and Michael J. Strain, "*High precision integrated photonic thermometry enabled by a transfer printed diamond resonator on GaN waveguide chip*", Opt. Express 29, 29095-29106 (2021). https://doi.org/10.1364/OE.433607

Steeneken, P.G., Dolleman, R.J., Davidovikj, D., Alijani, F. and van der Zant, H.S.J., 2021, "*Dynamics of 2D material membranes*", 2D Mater. 8 042001. https://doi.org/10.1088/2053-1583/ac152c

Walter Dickmann, Lukas Max Weituschat, René Eisermann, Stephan Krenek, Pablo Aitor Postigo, Stefanie Kroker, "*Heat dynamics in optical ring resonators*", Proceedings Volume 11783, Modeling Aspects in Optical Metrology VIII; 1178309 (2021). https://doi.org/10.1117/12.2592552

This list is also available here: https://www.euramet.org/repository/research-publications-repository-link